JOURNAL OF MATERIALS SCIENCE **36** (2001) 1943–1949

Finite element simulation of microindentation on aluminum

D. J. STRANGE, A. K. VARSHNEYA*
New York State College of Ceramics, Alfred University, Alfred, NY 14802, USA
E-mail: varshneya@alfred.edu

Vickers indentation of 6061-T6 aluminum was modeled using a three-dimensional finite element analysis (FEA) program. Two different work hardening behaviors were assumed. The results were compared with actual indentations using both a static microindenter and a load and depth recording microindenter. The hardness and plastic flow behavior showed excellent agreement, validating the FEA model, and implying that the work hardening of the aluminum decreases past a compressive strain of 0.09. The unloading results were analyzed using Sneddon's solution for the indentation of an elastic half-space by a rigid axisymmetric indenter. The results confirm the validity of applying Sneddon's solution in this case, implying that Bolshakov and Pharr's corrections of Sneddon's solution (which were determined for a conical indenter) are not directly applicable to the Vickers indenter.

1. Introduction

The understanding of load and depth sensing microindentation and nanoindentation tests for mechanical property analysis has made great strides during the last 15 years, in large part due to better analytical and finite element simulations of the elastic-plastic material response.

Traditionally, hardness tests such as the Vickers Hardness test have been used to simply calculate a hardness number which is characteristic of each material. This type of test allows comparison between different materials, and can be used for quality control purposes. It must be recognized, however, that Vickers Hardness is not a clearly defined material property but is instead a complex function of fundamental material properties such as elastic modulus, Poisson's ratio, yield stress, strain hardening, and time dependent plasticity. For certain materials additional factors such as surface energy, fracture toughness, pressure induced phase changes, anisotropic crystal structure, and grain size must be taken into account as well. The combination of all of these factors into one number, "VHN", creates a situation where it is impossible to back-calculate material properties from the indentation test.

The load and depth sensitive microindenter (dynamic microindenter) is a large improvement over the traditional static indenter. Monitoring load and depth during the indentation allows the calculation of additional hardness terms which, given suitable formula(s), could be used to calculate basic material properties. Unfortunately, the problem is complicated due to the complex inhomogeneous deformation of the indented material.

Until relatively recently these type of analyses relied heavily upon either semi-empirical formulas or analytical approximations. Some of the earliest work was performed by Tabor [1], who studied conical indentations in metals. At nearly the same time Hill [2] showed that, for perfectly rigid plastic materials (infinite elastic modulus)

$$H/\sigma_{\mathrm{y}} = \text{constant} \tag{1}$$

where H is the Vickers hardness and σ_y the plastic yield stress. This relationship does not apply to highly elastic materials or materials with strain hardening, however. This work was expanded by the experimental results of Hirst and Howse [3] who concluded that for wedge shaped indenters

$$H/\sigma_y = A + B\ln(E/\sigma_{\mathrm{y}}) \tag{2}$$

where A and B are constants and E is the Young's modulus.

Johnson [4] expanded the work of Tabor and came up with the equation

$$p_{\mathrm{av}} = \frac{2}{3}\sigma_{\mathrm{r}}\left(1 + \ln\frac{E\tan\psi}{3\sigma_{\mathrm{y}}}\right) \tag{3}$$

where σ_{r} is the flow stress in uniaxial compression which gives a plastic equivalent strain of 0.07, p_{av} is the average contact pressure (equivalent to "true" hardness) and ψ is the included angle of the indenter. Johnson took the angle ψ to be 19.7°, which gives the same volume of material displaced for a conical indentation as for a Vickers indentation. This formula works surprisingly well for materials with well defined constant strain hardening so long as neither significant pileup nor

* Author to whom all correspondence should be addressed.

"sinking in" of the material occurs. An attempt to account for the sinking in or piling up of the material was undertaken by Giannakopoulos *et al*. in 1994 [5]. With the aid of a finite element model (using a small-strain assumption), they derived

$$P=1.06h^2(\tan 22^\circ)^{-2}\sigma_u\left(1+\frac{\sigma_y}{\sigma_u}\right)\left(1+\ln\frac{E\tan 22^\circ}{3\sigma_y}\right). \quad (4)$$

where P is load, h is vertical displacement, and σ_u is the "ultimate" stress, which they defined as the stress at 30% plastic strain. In a paper by Zeng *et al*. [6], the same research group published the formula

$$P=1.19h^2(\tan 22^\circ)^{-2}\sigma_u\left(1+\frac{\sigma_y}{\sigma_u}\right)\left(1+\ln\frac{E\tan 22^\circ}{3\sigma_y}\right) \quad (5)$$

The later formula takes into account the results of a more accurate large-strain elastoplastic analysis. A similarly derived formula for the average contact pressure is

$$p_{av}=0.30\sigma_u\left(1+\frac{\sigma_y}{\sigma_u}\right)\left(1+\ln\frac{E\tan 22^\circ}{3\sigma_y}\right). \quad (6)$$

Equations 4–6 were deduced from curve-fitting of FEA results and were presented as being accurate for materials where $1\le\sigma_u/\sigma_y\le 3$ and $2\le\tan(90-\alpha)E/\sigma_y\le 30$ where α is the indenter angle measured from the vertical (i.e. 68° for a Vickers indenter). It should be noted that these equations, taken in the extreme of infinite yield stress (purely elastic), do not converge to the elastic solutions.

The above Equations 5 and 6 are the basis for a system developed by Zeng *et al*. for the determination of mechanical properties through indentation. This technique was applied to various brittle ceramic materials with some success [6].

The unloading portion of the curve is generally expected to follow the power law relationship

$$P=B(h-h_f)^m \quad (7)$$

where B and m are fitting parameters and h_f is the displacement after unloading. The instantaneous slope of the unloading curve, S, at the point of maximum load is therefore given by

$$S=\frac{dP}{dh}=mB(h_{max}-h_f)^{m-1}. \quad (8)$$

Knowing S, the Young's modulus of the material can then theoretically be derived by using the formula of Sneddon [7]

$$E_{eff}=\frac{E}{1-v^2}=\frac{S}{1.128\sqrt{A}} \quad (9)$$

where E_{eff} is the effective Young's modulus, E is the Young's modulus, v is Poisson's ratio, and A is the projected contact area. This formula was derived for an axisymmetric punch indenting an elastic half space, assuming small deformation. A refinement of the analysis was provided by R. B. King, who concluded that for a square punch (such as the Vickers diamond) the term 1.128 in Equation 9 should be replaced with 1.14 [8].

There exists some controversy as to the proper way to derive the projected contact area A from load vs. displacement data. The simplest way to derive A is by taking the displacement at maximum load and calculating the projected area based on the geometry of the indenter. The most commonly accepted method, however, is that suggested by Oliver and Pharr [9]. In their method the true effective contact area is assumed to be less than that given by the maximum depth (due to elastic "sinking in" of the material). Their method involves extrapolating the initial unloading slope to zero load and using that depth, h_c, to calculate the contact area. Estimates of Young's modulus calculated by this method are denoted E_{OP} in this paper. E_{area} denotes that the modulus was calculated using the true contact area as determined by FEA or direct observation.

1.1. Goals of the present analysis

It is the opinion of the authors that previous FEA indentation studies have not adequately demonstrated thorough agreement with experimental indentation data. Hence the primary focus of this study is on developing a more accurate FEA model and demonstrating close agreement with experimental static and recording Vickers indentations. 6061-T6 aluminum was chosen as an ideal subject material. 6061-T6 aluminum is well characterized, is largely strain-rate independent in its plasticity, and has a fine microstructure suitable for microindentation with an isotropic assumption. The demonstration of the accuracy of the FEA model on such a material is critical to any further investigations into materials that are not as well behaved or as well characterized. Furthermore, a demonstrably accurate FEA model allows for a critical evaluation of the formulae presently available in the literature for analysis of loading and unloading microindentation curves.

2. Experimental procedure

2.1. Finite element analysis

Finite element analysis was performed using the ANSYS version 5.6 software package running on the Windows NT platform. The material was treated as a homogeneous, isotropic, and rate-independent body with non-linear plasticity behavior on "VISCO107" type elements. This type of element uses 8 node brick elements and is specifically formulated to model large-strain isochoric (volume preserving) behavior. For the surface of contact, "CONTA173" surface to surface contact elements were used for the deformable material while a "TARGE170" element provided the diamond face, which was assumed to be perfectly rigid. The contact friction was assumed to be zero, which has been shown to be a reasonable assumption for the high-load test regime [10].

Plasticity behavior was modeled using multilinear isotropic hardening, which uses a von Mises stress yield criterion coupled with a user defined strain hardening curve and an associative flow rule. The actual equations solved are given in the ANSYS theory reference [11]. An iterative Newton-Raphson solution process was used (as necessitated by the non-linear behavior) with a minimum of 20 substeps specified during both the loading and unloading portions of the solution. The actual analyses used more than 20 substeps due to the adaptive descent feature of the ANSYS code which automatically bisects any substep which exceeds 10% plastic strain.

It should be noted that this type of elastic-plastic formulation, while accurate for large plastic strains, makes a hypoelastic assumption which is valid only for small elastic strains. Hence materials with very high hardness to Young's modulus (H/E) ratios will have less accuracy, and the FEA results will approach those solved using a "small strain" assumption. It is possible to increase the accuracy of the analysis by using a hyperelastic formulation. Hyperelastic constants for materials other than rubber are not easy to measure nor widely published, however. For aluminum, the H/E ratio is small and hence the error introduced from the hypoelastic assumption is negligible.

2.2. Plasticity data

The uniaxial compressive stress-strain curve for 6061-T6 aluminum was obtained from the results of Maiden and Green [12]. The uniaxial compression curve was translated to true tensile stress verses logarithmic strain using the relations $\tau = \sigma(1-\varepsilon_{\mathrm{p}})$ and $\varepsilon_{\mathrm{lp}} = -\ln(1-\varepsilon_{\mathrm{p}})$ where τ is the true tensile stress, σ is the uniaxial compression stress, ε_{p} is the plastic uniaxial compression strain, and $\varepsilon_{\mathrm{lp}}$ is the logarithmic plastic strain. The compression data of Maiden and Green ends at a strain of 0.09. Based upon previous work which indicated the possibility that higher strains may be obtained in the indentation process, the results of Maiden and Green were extrapolated in two different ways. For analysis "A" the behavior beyond 9% strain was assumed to be ideally plastic (no further strain hardening). In analysis "B" further strain hardening was assumed, with the slope of the stress-strain curve extrapolated to infinity as illustrated in Fig. 1. In both cases Young's modulus and Poisson's ratio were held constant at 70 GPa and 0.28, respectively.

2.3. Mesh geometry

The geometry of the mesh is shown in Figs 2 and 3. The model was built as a 45° slice of a cylinder, consistent with the eight-fold symmetry of the Vickers diamond. Appropriate symmetrical boundary conditions were applied. The model used 18018 solid elements. The radial and vertical dimensions of the model were 50 times the indentation depth to ensure that the behavior approximated that of a semi-infinite body. The validity of the assumption of semi-infinite body behavior was confirmed by increasing the size of the model. The results did not change significantly.

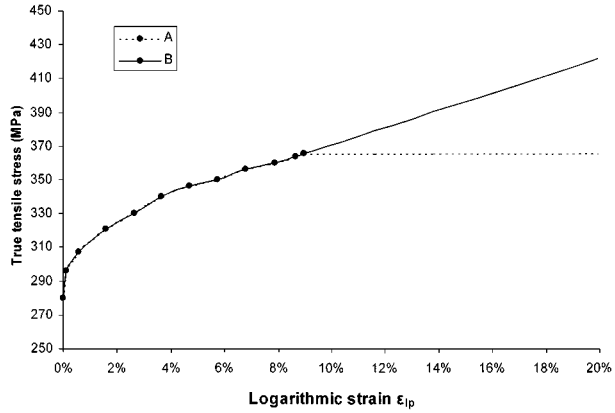

Figure 1 True tensile stress verses logarithmic strain for 6061-T6 aluminum showing two different work hardening assumptions.

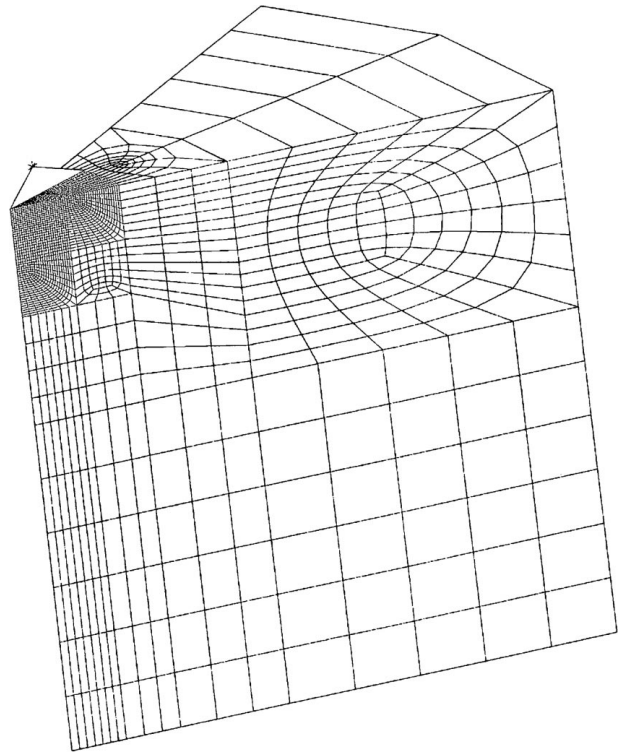

Figure 2 The finite element model used for the present analysis. One-eighth of the diamond indenter face is shown in contact with the specimen at the top left corner.

The indentation was applied to the model by driving the target element (representing the face of the diamond) vertically into the mesh to a distance of 200 μm. The properties of the material model do not allow for any load dependence of hardness, so the results of the 200 μm indentation can be extrapolated for any indentation depth.

2.4. Static indentations

A sample of polished 6061-T6 aluminum was indented, for comparison purposes, on a Buehler Micromet-II micro-hardness tester at loads of 1.96, 4.91, and 9.81 Newtons. The dwell time at load was 10 seconds. Three indentations were performed at each load. The resulting indentations were analyzed using a video microscope and image analysis software. Using this combination it

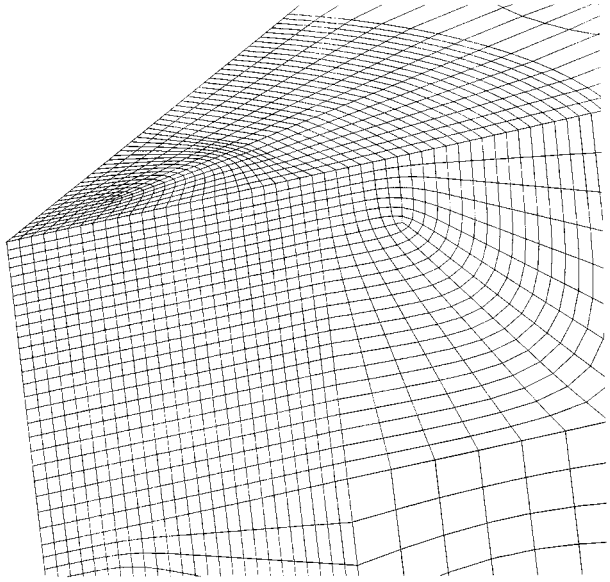

Figure 3 A close-up view of the region of the model near the tip of the indenter. The indenter itself has been removed from this view for clarity.

was possible to measure both traditional Vickers hardness (measured across the diagonal of the impression) and the "true" Vickers hardness (measured using the area of the indentation.)

2.5. Dynamic indentations

The 6061-T6 sample was also indented using a load and displacement sensing microindenter. The design, instrumentation, and calibration of this device is described in detail elsewhere [13]. Five indentations were performed to a maximum load of 4.6 Newtons at an indentation speed of 0.20 μm/sec. Dwell time at load was 10 seconds. The resulting data were corrected using a system compliance of 0.648 μm/N. This compliance factor was determined by "indenting" a large flat steel punch into a steel specimen. All of the resulting displacement in this case was assumed to be due to system compliance.

2.6. Indentation profiling

The indentations made with both the static and dynamic hardness testers were analyzed using a contact profilometer (Tencor P-10). In this technique a diamond probe is moved across the surface of the sample at a very low load and the displacement of the tip is measured. For these measurements a load of 5 mg was used and the tip speed was 10 μm/sec. The depth resolution was 1 μm. The direction of scan was at a 45° angle to the diagonal and centered on the impression. In this manner both an accurate total indentation depth and maximum height of material pileup can be measured.

3. Results and discussion

3.1. Terminology

A brief discussion of the nomenclature used to describe the results is in order. The traditional Vickers hardness number is given in units of kgf/mm^2 and is abbreviated "VHN". In accordance with the SI system of units this paper presents the results in GPa and hence "number" has been dropped from the name to yield VH. Subscripts denote deviations from the normal procedure for measuring the area of the indentation. VH_{face}, for example, indicates that the area was calculated by measuring the distance across the indentation faces and assuming that the indentation was square. The difference between VH_{face} and VH gives an indication of the degree to which the indentation deviates from a square. VH_{area} indicates that the area was measured directly.

Hardness computed from the load vs. displacement data at the point of maximum load (P_{max}) and maximum displacement (h_{max}) is referred to as loaded Vickers hardness (LVH). Hardness calculated using P_{max} and the unloaded displacement (h_f) is referred to as DVH [14]. "Pileup" is a measure of the maximum upward displacement of the material after unloading, expressed as a percentage of h_f.

There is the question of how to properly measure the indented area from the finite element analysis. During loading, the software allows a direct output of the projected area of those elements which exhibit contact. This area will be similar to, but slightly less than, that measured by calculating the area enclosed by the line of maximum upward displacement. After unloading the area can again be calculated by direct output of the projected area of the elements that had contact, or through observation of the positions of maximum displacement. It was determined that, after unloading, the second method more closely approximates the area which would be observed through a microscope after a real indentation. Hence this was the method which was used to calculate the area and the radial dimensions for VH_{area}, VH, and VH_{face}. During loading, however, the first method was used to find the area for Young's modulus calculations. The advantage of this method is that it gives the true area used by the ANSYS software to calculate the stiffness response.

3.2. Loading behavior

Fig. 4 shows the FEA load-displacement curves for the aluminum modeled with the two strain hardening methods, overlaid with the recording microindenter for aluminum. The FEA data has been scaled to a peak load of 4.6 Newtons so that it may be more easily compared to the experimental data. This scaling is only possible for the FEM data because it is truly load independent. Note that the proper way to scale this data requires a different scaling factor for each axis. The penetration axis is scaled by a constant, while the load axis is scaled by that constant squared. Various parameters derived from the FEA model and the recording microindenter experiments are summarized in Table I and Table II.

The two different strain hardening methods show only a relatively minor difference, indicating that the hardness is not *substantially* influenced by hardening at high strains (>0.09). This is in contrast to a previous finite element analysis of Giannakopoulos *et al.* [4] in which they found that a constant hardening tangent increased the hardness by nearly 50%. It is however in

TABLE I Aluminum material properties calculated from the finite element model and the recording microindenter

	No hardening "A"	Constant hardening "B"	Recording indenter (load 4.6 N)
Pileup (%)	19.7%	15.4%	$19 \pm 2\%$ [a]
LVH (GPa)	1.04	1.06	1.04 ± 0.02
DVH (GPa)	1.22	1.24	1.23 ± 0.03
h_f/h_{max}	0.925	0.925	0.90 ± 0.01
E_{OP}/E_{true} [b]	1.23	1.16	1.86 ± 0.09
E_{area}/E_{true} [b]	1.05	1.03	1.74 ± 0.09
VH_{area} (GPa)	0.89	0.95	0.99 ± 0.01 [c]
VH_{face} (GPa)	0.83	0.82	0.91 ± 0.04 [c]
VH (GPa)	1.00	1.02	1.13 ± 0.04 [c]

[a] Indentations from the recording microindenter measured using the contact profilometer.
[b] True (input) elastic modulus is 70 GPa.
[c] Indentations from the recording microindenter measured using the video microscope.

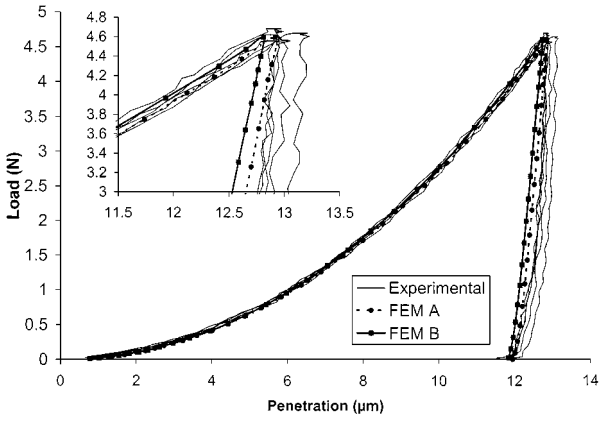

Figure 4 6061-T6 aluminum load verses displacement data. Five experimental recording microindenter runs are shown combined with data from the two FEM analyses. The inset shows a more detailed view of initial unloading region. The FEM data has been scaled to a peak load of 4.6 N.

good agreement with Equation 3, which predicts that the hardening only up to a strain of 0.07 is significant. One significant difference between the two FEA models is that model "B" (with constant strain hardening) exhibited less pileup. Intuitively this makes sense, as significant pileup requires large plastic strains of the material close to the indented surface. Work hardening at high strains impedes this process.

Average contact pressure p_{av} calculated using Equation 3 and the corresponding E, σ_y, and σ_r values

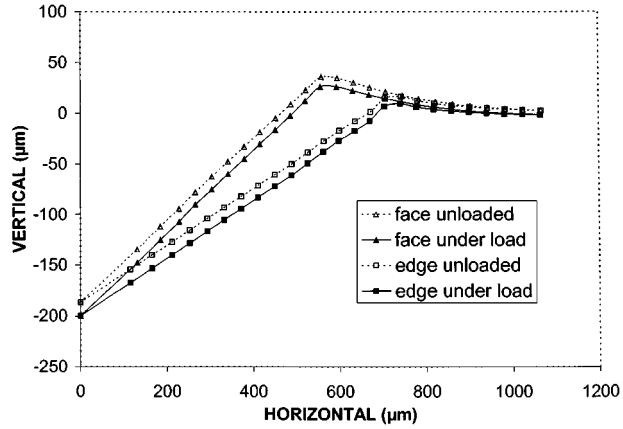

Figure 5 The vertical displacement at the edge and face of model "A". The elastic recovery occurs primarily in the vertical direction.

(70 GPa, 280 MPa, and 354.8 MPa respectively) is 1.04 GPa. Average contact pressures from the FEA (using P_{max} and the true projected contact area) are 0.93 and 1.03 GPa for runs *A* and *B* respectively. There are no experimental measurements which correlate directly to p_{av} due to the fact that true projected contact area cannot be measured during loading. However the finite element model indicates that *the area of indentation does not change significantly upon unloading*; the elastic recovery occurrs primarily in the vertical direction as shown in Fig. 5. Hence VH_{area} can be expected to closely approximate p_{av}.

LVH values calculated using Giannakopoulos *et al.*'s Equation 5 and assuming σ_u to be 365 and 473 MPa (corresponding to FEA models "A" and "B") are 0.76 and 0.83 GPa respectively. These value are significantly too low; however, it must be said that the value of $\tan(90 - \alpha)E/\sigma_y$ lies outside the valid range for this equation given in reference [6].

Model "A", with no strain hardening past a strain of 0.09, is a closer match to the experimental data in every respect. The plastic height (pileup), LVH, and VH_{area} all match the experimental data very closely. Model "B", which has a constant strain hardening tangent, exhibits hardness values which could also be construed as being in rough agreement with the experimental values. Model "B" has a significantly lower plastic height, however. It must be concluded that model "A" is a more accurate model of the true strain hardening behavior of 6061-T6 aluminum.

TABLE II Contact profilometer and video microscope data for the aluminum samples indented using the static indenter

		contact profilometer			video microscope		
Sample	Load N	Pileup height (%)	VH_{face} GPa	DVH GPa	VH GPa	VH_{face} GPa	VH_{area} GPa
6061-1	9.81	22.22%	0.780	1.414	1.127	0.902	0.974
6061-2	9.81	16.99%	0.825	1.431	1.115	0.872	0.959
6061-3	9.81	18.21%	0.841	1.414	1.114	0.879	0.962
6061-4	4.90	21.08%	0.767	1.506	1.143	0.852	0.964
6061-5	4.90	21.81%	0.787	1.453	1.186	0.815	0.955
6061-6	1.96	20.87%	0.757	1.559	1.186	0.850	0.953
6061-7	1.96	19.78%	0.789	1.559	1.129	0.879	0.988
6061-8	1.96	17.03%	0.823	1.559	1.128	0.972	1.005
average		19.75%	0.796	1.487	1.141	0.878	0.970
standard deviation		2.10%	0.030	0.066	0.029	0.046	0.018

TABLE III Size of the zone of plastic deformation for models "A" and "B", expressed as a function of h_{max}

	Model "A"	Model "B"
Along the edge	$6.46 \cdot h_{max}$	$6.53 \cdot h_{max}$
Along the face	$6.38 \cdot h_{max}$	$6.72 \cdot h_{max}$
Vertical	$7.33 \cdot h_{max}$	$7.67 \cdot h_{max}$

3.3. Plastic zones

The dimensions of the zone of plastic deformation were found to deviate only slightly from hemispherical, being slightly deeper than wide. Model "B" has a larger plastic zone than "A", as illustrated by Table III which expresses the dimensions of the plastic zone scaled to the total indentation depth h_{max}. Previous work has shown that work hardening has a tendency to drive the plastic zone to greater depths [15]. The present work shows that, in this case, additional work hardening also slightly expands the radius of the plastic zone.

3.4. Unloading behavior

While both FEA curves agree quite well with the experimental results during the loading portion, there are some discrepancies in the unloading cycle. The experimental curves exhibit greater curvature towards the end of the unloading cycle and slightly less curvature in the initial portion. The net effect yields a higher calculated elastic modulus for the experimental curve. Some of this difference may be attributable to inertial effects caused by the mass of the indentation column. It is also possible that the indentation stage and frame do not perform exactly as ideal Hookean springs, but rather exhibit some non-ideal elastic or even viscoelastic behavior. Whatever the cause, the short distance over which the aluminum recovers exacerbates the problem and increases the sensitivity of the unloading results to the correction factor.

It is useful to compare the elastic modulus derived from the FEA load vs. displacement value with the elastic modulus input into the model. The ratio of the two provides an indication of the accuracy of Sneddon's solution. When the modulus is calculated using the Oliver-Pharr method the calculated values are 23% and 16% too large for models A and B respectively. This is not unexpected because the Oliver-Pharr method assumes that there is sinking-in of the material instead of pileup. Therefore, for a highly plastic material such as aluminum, the Oliver-Pharr method can be expected to underestimate the true contact area. When the true contact area is taken into account the calculated modulus is larger than the true modulus by only 3.7% and 0.1%.

Some insight into the causes of overestimation of Young's modulus is provided by the work of Bolshakov and Pharr [15]. Their finite element model used a conical indenter for the advantage in processing time, which allowed them to examine hypothetical materials over a range of yield stresses both with and without work hardening. In their analysis they assumed work hardening to be linear with strain, with a slope equal to $10\sigma_y$. They found it useful to classify the different material responses according to the ratio h_f/h_{max}, the ratio of the unloaded depth to the depth at maximum load. For $h_f/h_{max} < 0.7$, they found the FEM estimation of E_{area}/E_{input} to be consistently 5–10% too high. They attribute this difference to an inaccuracy in Sneddon's solution and, in a separate paper [16], treat the problem analytically. The correction they derived for a conical indenter is

$$E_{eff} = \frac{E}{1-\nu^2} = \frac{1}{\beta}\frac{\sqrt{\pi}}{2}\frac{S}{\sqrt{A}}$$

where

$$\beta = 1 + \frac{(1-2\nu)}{4(1-\nu)}\left(3 - \frac{\pi}{2}\right)\cot(\phi) \qquad (10)$$

Taking the indenter angle ϕ as 70.3° (giving the same area to depth relationship as the Vickers diamond) and $\nu = 0.28$, the correction to Sneddon's formula, β, is 1.078. This correction does not account for the FEA estimation of E_{area}/E_{input} when $h_f/h_{max} > 0.7$ however. Bolshakov and Pharr found that in this regime the E_{area}/E_{input} values increases with increasing h_f/h_{max}. For $h_f/h_{max} = 0.93$ (corresponding to the present analysis of aluminum) they found the error to be 15% and 13% for zero strain hardening and constant strain hardening (at $\nu = 0.25$). When one corrects these values to $\nu = 0.28$, assuming that the results will scale in the same ratio as Equation 10, the errors decrease to 14% and 12% respectively. This correction is much higher than the small discrepancy showed by the present analysis. Hence the corrections derived by Bolshakov and Pharr for a conical indenter are shown by the present study to be inapplicable to a true three-dimensional Vickers indentation in aluminum.

3.5. Indentation shape

Although models "A" and "B" had nearly identical hardness values, there is a significant difference in the degree of pileup. Fig. 6 shows the indentation shapes after unloading. The viewing plane bisects two faces of the indentation, the plane showing the highest amount of pileup. In this figure the FEA data has been scaled to

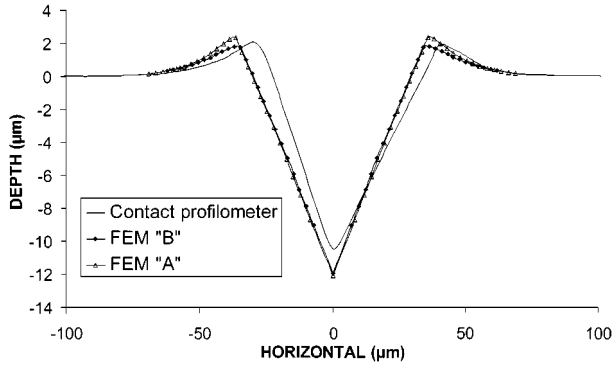

Figure 6 Unloaded indentation shapes perpendicular to the pyramid faces for the two FEM models and the a representative contact profilometer trace. The FEM curves have been scaled so that the peak loads are the same (4.6 N).

the same peak load as the indentations done with the recording microindenter (4.6 N). Representative data from the contact profilometer is included. The contact profilometer data is not perfectly symmetrical, this being due to side-loading forces on the profilometer tip as it moves down and then up the wall of the indentation. These forces (known as arcal error) have a tendency to steepen the downward slope, as the diamond tip is bent in the direction of motion, and flatten the upward slope. In Fig. 6 the scan direction is from left to right.

Additionally, the profilometer is not able to adequately capture the very sharp tip of the indentation and hence this point must be inferred by extrapolation. When this is done the unloaded depth h_f from the profilometer is close to, but still less than, the FEA depth despite the similarity in indentation width. Actually, this difference in h_f affects the reported pileup values, which are given as a percentage of h_f. Because of this, the tabulated values of pileup indicate that model "A" is a very close match to the experimental results. However, when the pileup is considered as a function of load instead of h_f, the experimental pileup lies between models "A" and "B".

4. Conclusions

In this paper we have presented results for a new three-dimensional FEA numerical model of Vickers indentation applied to 6061-T6 aluminum. Using only the known elastic properties and compressive stress-strain data a reasonably accurate portrait of the indentation process has been drawn. The agreement with experimental static and recording indentation data is excellent, particularly during the loading cycle, and the shape of the unloaded indentation given by the FEA is nearly identical to that measured using contact profilometry. The FEA model confirmed that elastic recovery upon unloading occurs primarily in the z (depth) direction. The discrepancies between the FEA and the experimental data observed during the unloading portion of the P-h curve are minor and may be ascribed to small instrumental errors.

Varying the work hardening behavior of the material input into the FEA model at strains greater than 0.09 showed only a minor effect on the hardness, in sharp disagreement with some previous FEA work by Giannakopoulos *et al*. The cause of the discrepancy is unknown at this time and is expected to be addressed in later work.

Analysis of the P-h curve at unloading demonstrates that Sneddon's solution for calculating Young's modulus can be accurate even for highly plastic materials, but only if the appropriate area of contact is used in the calculation. The present methods for determining this area of contact from the P-h curve are insufficient for materials such as aluminum which exhibit significant piling up of material at the indentation edges.

Acknowledgements

The authors would like to thank the Center of Advanced Ceramic Technology at Alfred University and Saxon Glass Technologies, Inc, Alfred NY 14802 for financial support.

References

1. D. TABOR, "Hardness of Metals" (Chapman & Hall, London, 1951).
2. R. HILL, "The Mathematical Theory of Plasticity" (Clarendon Press, Oxford, 1950).
3. W. HIRST and M. G. J. W. HOWSE, *Proc. Roy. Soc.* **A311** (1969) 429.
4. K. L. JOHNSON. *J. Mech. Phys. Solids* **18** (1970) 115.
5. A. E. GIANNAKOPOULOS, P. L. LARSSON and R. VESTERGAARD, *Int. J. Solids Str*. **31** (1994) 2679.
6. K. ZENG, E. SÖDERLUND, A. E. GIANNAKOPOULOS and D. J. ROWCLIFFE, *Acta Mater*. **44** (1996) 1127.
7. I. N. SNEDDON, *Int. J. Engng. Sci*. **3** (1965).
8. R. B. KING, *Int. J. Solids Str*. **23** (1987) 1657.
9. G. M. PHARR, W. C. OLIVER and F. R. BROTZEN, *J. Mater. Res*. **7** (1992) 613.
10. H. LI, A. GHOSH, Y. H. HAN and R. C. BRADT, *ibid*. **8** (1993) 1028.
11. ANSYS 5.6 theory reference 4.1.8.
12. C. J. MAIDEN and S. J. GREEN, *J. App. Mech*. **88** (1966) 496.
13. W. MASON, P. F. JOHNSON and J. R. VARNER, *J. Mater. Res*. **7** (1992) 3112.
14. A. K. VARSHNEYA, in Proceedings of the 4th Brazilian Symposiun on Glasses and Related Materials, Ouro Preto, Brazil, November 1999, *J. Non-Cryst. Sol.* **273** (2000) 1.
15. A. BOLSHAKOV and G. M. PHARR, *J. Mater. Res*. **13** (1998) 1049.
16. *Idem*., *Mat. Res. Soc. Symp. Proc*. **436** (1997) 189.

Received 8 March
and accepted 24 October 2000